Chapter 3
Range and Doppler Tracking Observables

3.1 The Tracking Link

Communications from Earth to spacecraft and from spacecraft to Earth are made within internationally allocated frequency bands [1], as shown in Table 3-1:

Table 3-1. Uplink and downlink frequencies for deep-space communications.

Band	Uplink Frequency (MHz)	Downlink Frequency (MHz)
S	2110–2120	2290–2300
X	7145–7190	8400–8450
Ka	34,200–34,700	31,800–32,300

The Deep Space Network (DSN) developed S-band capability for uplinks and downlinks in the 1960s. In the mid-1970s, spacecraft were equipped with dual-frequency S/X downlinks. (Signals at the two downlink bands are coherent with each other, having been derived from the same reference signal.) In 1989, an X-band uplink capability was added. The Magellan spacecraft was the first to use this capability and could transmit coherent S/X downlinks that were derived from an X-band uplink. Most spacecraft launched in the 1990s transmit and receive at X-band only. Cassini, however, can operate with an X-band uplink and coherent X/Ka downlinks. Further use of Ka-band is planned for the 21st century. The move toward higher frequencies is largely driven by the desire for better communications performance, but higher frequencies also improve the accuracy of radiometric measurements by using shorter wave-

lengths and by reducing effects due to charged particles in the ionosphere and solar plasma.

Spacecraft range is measured by the round-trip transit time of a ranging signal generated at one of the DSN stations (located at Goldstone, California; Canberra, Australia; and Madrid, Spain). A ranging signal, consisting of a sequence of sinusoidal tones derived from the station frequency standard, is phase modulated onto the transmitted carrier signal [2]. The spacecraft receiver locks on and tracks the uplink carrier via a phase-locked loop that produces a reference signal coherent with the uplink carrier. This reference signal is used to demodulate the ranging signal, which is then passed through a lowpass filter, currently with an upper cutoff frequency of less than 2 MHz. The ranging signal is phase modulated onto the downlink carrier, a signal coherent with the uplink but offset in frequency. (For example, assuming an X-band uplink, the downlink frequency would be higher by a factor of 880/749 at X-band and 3344/749 at Ka-band.) A phase-locked loop at the receiving station produces a reference signal coherent with the received signal. This reference signal is used by the ranging assembly to demodulate the downlink signal. The received range code is compared against a model of the transmitted range code to determine the round trip transit time. Range measurements are quantized in steps referred to as range units (RU). The size of an RU depends on the frequency of the highest component of the code, and is currently about 28 cm. Doppler data are obtained by differencing the received reference signal with the station frequency reference.

A new ranging capability is being added to future flight systems. It will use a pseudo-random noise code rather than a sequence of tones. This code will be detected and regenerated onboard the spacecraft. Using this code will ensure more efficient use of the downlink power because only the range code will be modulated onto the carrier, rather than a 2-MHz noise passband, thus enabling ranging measurements to be made at greater distances and at lower signal levels [3].

Spacecraft topocentric (slant) range (see Fig. 3-1) is approximately related to the one-way signal transit time, τ_g, by the expression

$$\rho = \tau_g c \tag{3.1-1}$$

where c is the speed of light. An approximate expression for the received frequency from a spacecraft receding from Earth is

$$f_R = \left(1 - \frac{\dot{\rho}}{c}\right) f_T \tag{3.1-2}$$

where f_T is the frequency transmitted by the spacecraft and $\dot{\rho}$ is the spacecraft instantaneous slant range rate. The quantity $(\dot{\rho}/c)f_T$ is referred to as the

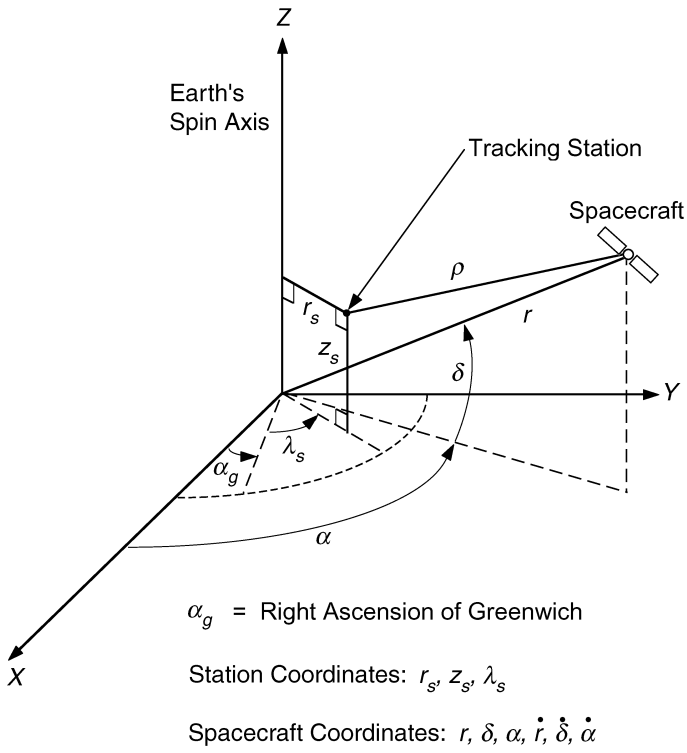

Fig. 3-1. Spacecraft and station coordinates.

Doppler shift. The Doppler measurement thus provides information on the spacecraft topocentric range rate.

A simplified illustration of the Doppler extraction process is given in Fig. 3-2. A Doppler counter measures the total phase change with resolution better than one one-hundredth of a cycle during a count time, T_c. Each time the phase of the received signal slips one cycle relative to the phase of the transmitted signal, the distance over which the signal has propagated has increased by one wavelength, or 3.6 cm at X-band. The Doppler count thus provides a measure of range change over T_c.

The most accurate ranging and Doppler measurements are obtained via a two-way tracking mode for which the transmitting and receiving stations, and hence the frequency standards, are the same. For some missions, this configuration is impossible due to the extraordinary distances. For example, the round-trip light time (RTLT) of Voyager 2 at Neptune exceeded 8 hours. In such geometries, the transmitting station can rotate out of sight of the spacecraft by the time the signal returns to Earth, and thus, a second station is

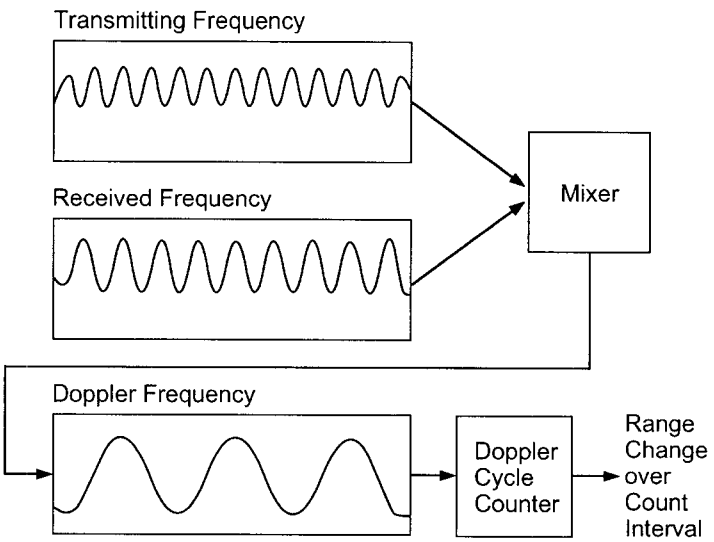

Fig. 3-2. Doppler extraction process. The difference between the transmitted and received carrier frequencies yields the Doppler tone. A cycle counter measures phase change of the Doppler tone, yielding a measure of range change during the count interval.

required to receive. This situation is referred to as three-way tracking. A third option is termed one-way tracking, in which the spacecraft generates a downlink signal from an onboard oscillator. In this mode, there is no transmission to the spacecraft.

One-way, two-way, and three-way tracking modes may be used at various times during a mission. The radiometric data obtained from each mode must be carefully modeled to account for uplink and downlink geometry, transmitting frequencies, spacecraft delays, relativistic, and other effects discernible in the residuals [4]. In the two-way mode, for example, the frequency transmitted at the spacecraft is a Doppler-shifted replica of the uplink frequency. Hence, the measured Doppler shift one RTLT later is approximately $(2\dot{\rho}/c)f_T$.

3.2 Range and Doppler Information Content

The spacecraft and station geometry at any instant of time is illustrated in Figs. 3-1 and 3-3. The slant range rate, $\dot{\rho}$, from the tracking station to a distant spacecraft can be closely approximated [5] by the expression

$$\dot{\rho}(t) = \dot{r}(t) + \omega_e r_s \cos\delta \sin(\omega_e t + \phi + \lambda_s - \alpha) \qquad (3.2\text{-}1)$$

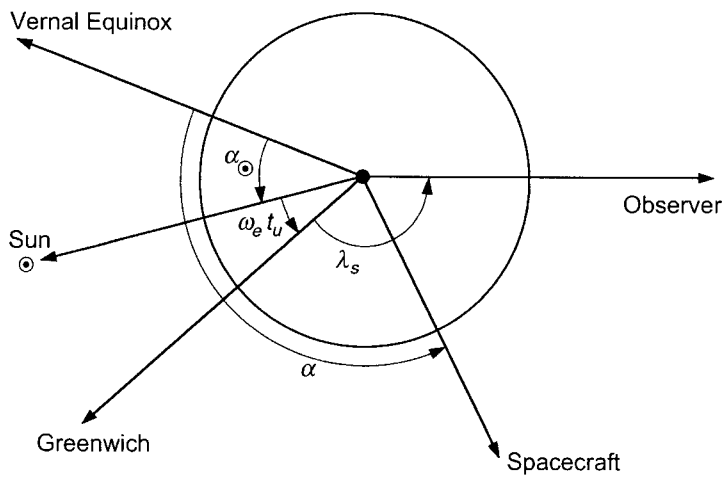

Fig. 3-3. Equatorial projection of coordinates.

where

$\dot{r}$ = geocentric range rate

ω_e = mean rotation rate of Earth

r_s = distance of tracking station from Earth spin axis

λ_s = longitude of tracking station

α = right ascension of spacecraft

δ = declination of spacecraft

ϕ = phase angle that depends on the epoch.

When time, t, is expressed as universal time (civil time at Greenwich), then ϕ is the instantaneous right ascension of the mean Sun.

As depicted in Fig. 3-4, the range rate observable given in Eq. 3.2-1 is essentially a sinusoid superimposed upon a ramp function representing the spacecraft geocentric velocity. The diurnal modulation is the result of the rotation of the tracking station about Earth's spin axis. The amplitude and phase of this modulation provide information about the spacecraft declination and right ascension. Notice, however, that accurate determination of these parameters depends not only upon the precision of the range rate observation, but also upon the accuracy to which the model parameters such as the tracking station locations and Earth orientation are known. For example, an error in station lon-

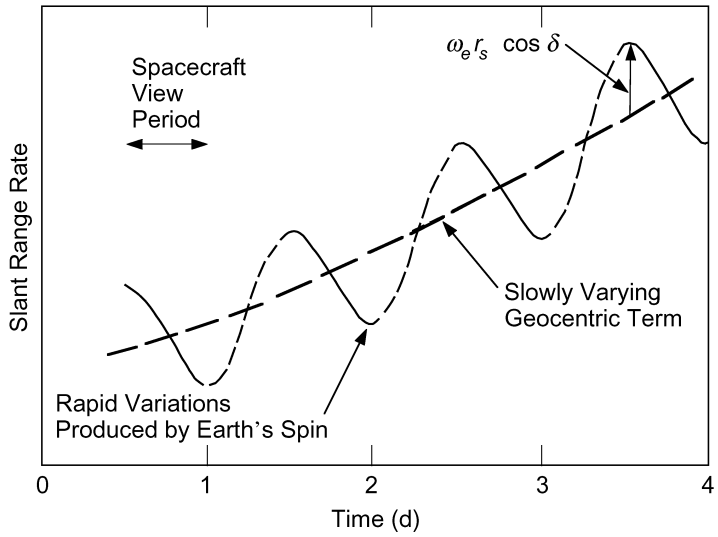

Fig. 3-4. Schematic illustration of idealized Doppler observable.

gitude maps one-for-one into an error in spacecraft right ascension. A detailed description of major Doppler modeling errors is given in the next section.

Doppler data are typically recorded continuously during the tracking pass at each DSN complex. From a single pass of Doppler, it is possible to determine spacecraft radial velocity, right ascension, and declination. Velocities normal to the line of sight can be inferred from several days or more of Doppler data [6]. Geocentric range can also be inferred from spacecraft accelerations observed in multiple passes of Doppler through constraints imposed by solar system gravitational force models.

Although orbit determination strategies have traditionally relied upon continuous Doppler passes to infer spacecraft angular position, there are significantly more powerful methods such as VLBI for measuring angles and angle rates directly. These will be discussed in Chapter 4. It should also be pointed out that range data, if continuously acquired, have a time signature similar to those for Doppler and provide spacecraft angular information as well as geocentric range and range rate. In fact, several days of continuous, biased range data with an accuracy of 1 m have the same angular information as a comparable track of Doppler with an accuracy of 0.1 mm/s.[1] The complementary information in range and Doppler observations can be useful in identifying poorly modeled spacecraft accelerations. This situation is explored further in Section 3.6.

[1]T. P. McElrath, personal communication, Navigation and Flight Mechanics Section, Jet Propulsion Laboratory, Pasadena, California, July 2000.

3.3 Tracking Data Error Sources

A number of errors in the Doppler and range observations limit the accuracy to which spacecraft orbits can be determined. For example, errors in the tracking equipment, such as clock instabilities and instrumental delays of signals, degrade accuracy. In addition, the transmission media introduce delays and dispersions into signals. Further, imperfect models of the tracking geometry, due to errors in station locations or Earth orientation, limit the ability to estimate spacecraft position. In this section, we explore the sensitivity of the Doppler and range data to current major sources of error in observable models, and we discuss means for calibrating, or removing, these errors.

3.3.1 Clock Instability

A fundamental source of error in radiometric tracking is clock instability. Consider the Doppler extraction process in Fig. 3-2. The received signal is beat against (mixed with) a local frequency reference. Any offset of this frequency reference from the actual transmitted frequency (either originating on the ground or on the spacecraft) will translate into an error in range rate. For example, in the one-way transmission mode, an oscillator onboard the spacecraft generates a reference signal that is transmitted by the spacecraft and received on the ground. The most stable space-qualified crystal oscillators currently available fluctuate about one part in 10^{13} over averaging intervals of 1000 seconds.[2] Over the longer time intervals important to navigation performance, crystal oscillator stability is generally worse. An unknown constant frequency offset of Δf relative to the nominal frequency, f, translates into a range rate measurement error of

$$\Delta\dot{\rho} = c\frac{\Delta f}{f} \tag{3.3-1}$$

As we shall see, a frequency offset larger than 10^{-13} is a major error relative to the best Doppler systems operating today. In the two-way tracking mode, the frequency standards associated with the transmitter and receiver are identical and, furthermore, a highly stable standard, such as the hydrogen maser, is typically used. These frequency standards are stable to a few parts in 10^{15} over a typical RTLT [7]. To understand how the frequency standard affects a two-way Doppler measurement, a short discussion of frequency stability is necessary.

The accepted measure of stability of frequency standards in the time domain is the two-sample Allan variance with no dead time [8]

---

[2] S. W. Asmar, personal communication, Communications Systems and Research Section, Jet Propulsion Laboratory, Pasadena, California, June 2000.

$$\sigma_y^2(\tau) = \frac{1}{2} < (\bar{y}_{k+1} - \bar{y}_k)^2 > \tag{3.3-2}$$

where $\bar{y}_k$ and $\bar{y}_{k+1}$ are adjacent measurements of fractional frequency deviation, with averaging time, τ. The brackets denote ensemble averaging. The fractional frequency deviation is computed by subtracting the clock phase error at the beginning of the averaging interval from the phase error at the end of the averaging interval, and then dividing by the product of the nominal frequency times the averaging interval. The range rate error for a count time, τ, and RTLT of $M\tau$ is given by [9]

$$\Delta\dot{\rho} = c(\bar{y}_{k+M} - \bar{y}_k) \tag{3.3-3}$$

The root-mean-square (rms) error is given by

$$c < (\bar{y}_{k+M} - \bar{y}_k)^2 >^{1/2} = \sqrt{2}\, c\sigma_y(2, M\tau, \tau) \tag{3.3-4}$$

where $\sigma_y^2(2, M\tau, \tau)$ is the two-sample Allan variance with averaging time, τ, and sample interval, $M\tau$. The Doppler error thus depends on the Allan variance at time scales of between τ and $M\tau$. Approximations of this general form of the Allan variance can be made in terms of the usual two-sample Allan variance with no dead time for several types of noise that are common for frequency standards. The DSN hydrogen masers exhibit white frequency noise at time scales of 60 to 1000 s, and they exhibit flicker frequency noise at time scales of 1000 s to about 12 hours [7]. For a Doppler count time, τ, which is less than the RTLT, which is itself less than 1000 s, the range-rate error due to frequency instability is given by

$$c < (\bar{y}_{k+M} - \bar{y}_k)^2 >^{1/2} = \sqrt{2}\, c\sigma_y(\tau) \tag{3.3-5}$$

while for a Doppler count time of τ and an RTLT of between 1000 s and 12 h, the error is approximately given by

$$c < (\bar{y}_{k+M} - \bar{y}_k)^2 >^{1/2} \approx \sqrt{2 + \log_2 M}\, c\sigma_y(\tau) \tag{3.3-6}$$

where M = RTLT/τ. The Allan standard deviation, $\sigma_y(\tau)$, of the DSN hydrogen masers is typically about 8×10^{-15} for $\tau = 60$ s,[3] and about 1×10^{-15} for $\tau = 1000$ s [7]. This effect is negligible relative to other errors in the system such as troposphere (see Section 3.3.3).

---

[3] R. L. Tjoelker, personal communication, Tracking Systems and Applications Section, Jet Propulsion Laboratory, Pasadena, California, May 2000.

Notice that for Doppler measurements, frequency stability requirements are more stringent than timing requirements. The clock epoch provides only the observable time-tag. For example, for a spacecraft in cruise, a time-tag error of 1 μs would translate into a negligible right ascension error of less than 0.1 nrad, as inferred from the Doppler signature (see Eq. 3.2-1). Doppler measurements from a planetary orbiter, such as Mars Global Surveyor (MGS), are sensitive to clock epoch at the microsecond level, however. The Doppler error $\Delta\dot{\rho}$ arising from a station clock epoch error ΔT is given by

$$\Delta\dot{\rho} = \ddot{\rho}\Delta T \tag{3.3-7}$$

Given a station clock error of 2 μs, a barely discernible Doppler measurement error of 0.016 mm/s would result for a short-period (or eccentric) orbiter accelerating at 8 m/s^2. While this size error would be difficult to detect in Doppler acquired from a single station, it could be revealed in Doppler data acquired simultaneously at two stations. Microsecond-level clock synchronization of the DSN clocks relative to UTC, routine now for about three decades, keeps this error at an insignificant level.

The effect of clock instability on two-way range data is approximately

$$\Delta\rho = \sqrt{2}\, c\tau\sigma_y(\tau) \tag{3.3-8}$$

where τ is the RTLT. With hydrogen maser stability, this effect is negligible—about 1 mm at one astronomical unit (AU) (for example, at Mars). However, clock epoch offsets between the transmitting and receiving stations can be a major error source for three-way ranging. In this case, the effect is approximately given by

$$\Delta\rho = c\Delta T \tag{3.3-9}$$

where ΔT is the clock offset. Thus, an unknown offset of 10 ns would result in a significant range error of 3 m.

The DSN has been using techniques such as observations of signals from the Global Positioning System (GPS) satellites to measure clock offsets over intercontinental distances to about the 10-ns level. Station calibrations are then required to relate tracking data time tags to station time at the clock reference point. Current calibration accuracy is about 1 μs. The GPS tracking system calibration method has the potential for near real-time clock offset measurements at the 1-ns level [10–12]. However, the navigation benefits of GPS clock calibration will be realized only if improved methods are developed to: (a) translate GPS measurement time to station time and (b) calibrate spacecraft tracking

signal path delays from the antenna front end to the baseband signal processor. The GPS calibration system is described in Section 3.4.

Although range measurements are highly sensitive to clock epoch offsets between transmitting and receiving stations, they are relatively insensitive to time-tag errors. An unknown time-tag error of ΔT would result in a range error of approximately

$$\Delta\rho = \Delta T\dot{\rho} \tag{3.3-10}$$

Thus, a time-tag error of 1 μs would result in a range error of 4 cm at a typical range rate of 40 km/s. A clock rate offset of $\Delta\dot{T}$ would result in a two-way range error of

$$\Delta\rho = c\mathrm{RTLT}\Delta\dot{T} \tag{3.3-11}$$

This effect is also small for spacecraft traveling in the inner solar system; an unknown clock rate offset of 10^{-13} causes an 11-cm range error for a one-hour RTLT.

The DSN has implemented a new frequency standard in the network, referred to as the linear ion trap standard, or LITS. This standard, when coupled with a cryogenically cooled, compensated sapphire oscillator (CSO) promises higher stability at all averaging times than the hydrogen maser [13]. Short-term stability of $3 \times 10^{-14}/\tau^{1/2}$ is achieved with the CSO, coupled with a long term stability of 6×10^{-16} or better (for $\tau > 10{,}000$ s) demonstrated by the LITS [13,14]. The first CSO will be installed at the Goldstone Deep Space Station by the end of 2000 to support the Cassini Ka-band radio science experiment [15]. Implementation at the Spain and Australia stations will be completed by the end of 2002. Once this implementation is successfully completed, the hydrogen masers will be retired from operation.[4]

3.3.2 Instrumental Effects

Limitations in station instruments arising from such factors as fundamental physics, design trade-offs, and the need for multipurpose functionality result in both random and systematic measurement errors. Random errors are caused by thermal noise, which is proportional to the receiver operating temperature and introduces a purely white noise into each measurement. Systematic errors are caused by dispersive and nondispersive instrumental delays and by antenna multipath.

The contribution of these errors to observable accuracy is highly measurement dependent. For example, group delays in the station and spacecraft elec-

[4]R. L. Tjoelker, personal communication.

tronics currently represent the major source of error in the ranging system. Uncalibrated delays of 13 ns or more in the two-way path may occur, producing biases of about 2 m in the inferred one-way range. System noise effects, on the other hand, depend largely on spacecraft transmitter power, and typically fall in the range of 10 to 100 cm with present day 2-MHz ranging systems [16].

Doppler measurement errors due to instrumentation result primarily from thermal noise and instabilities in the signal path through the receiver and exciter subsystems and the spacecraft transponder. Uncalibrated instrumental effects currently contribute about 0.003 mm/s to Doppler measurement errors for a 60-s count time.

3.3.3 Transmission Media

Charged particles in the interplanetary medium and Earth's ionosphere cause dispersive propagation delays in interplanetary radio signals. These frequency-dependent effects cause a group delay that can be closely approximated as

$$\Delta\tau_g = \frac{k}{f^2}, \quad k > 0 \tag{3.3-12}$$

Thus, a ranging code modulated on the carrier signal will experience a positive delay. Carrier phase, on the other hand, is advanced so that the phase delay is approximately

$$\Delta\tau_\phi = -\frac{k}{f^2} \tag{3.3-13}$$

The constant, k, is proportional to the total electron count (TEC) per unit area along the signal path through the ionosphere and solar plasma. The effective signal delay then depends upon the time of transmission during the Sun cycle as well as the signal ray path relative to the Sun. In addition, the ionospheric delay also varies diurnally and seasonally. The magnitude of the ionospheric effect at X-band during the daytime is approximately 20–60 cm at zenith. The nighttime effect is typically less by an order of magnitude. Furthermore, there is an elevation angle dependence that varies from a factor of one at zenith to a factor of three at the lowest elevations.

Solar plasma delays at X-band can range from 1 m to 75 m, depending largely upon how angularly nearby the Sun the signal travels. For a Sun-Earth-probe angle of 20 deg, the plasma delay at X-band typically drifts by about 1 m over an 8-h tracking pass. This effect was calculated by Kahn[5] based upon propagation observations of Woo and Armstrong [17] and Coles and

[5]R. D. Kahn, personal communication, Tracking Systems and Applications Section, Jet Propulsion Laboratory, Pasadena, California, August 1991.

Harmon [18]. Variability in solar conditions can cause the actual drift to vary by up to an order of magnitude from the mean.

The frequency dependency of charged particle delays allows for nearly complete cancellation of these effects for spacecraft with dual-frequency radio systems, for example, S- and X-band. Note, however, that this approach requires dual-frequency uplink and downlink transmissions for two-way Doppler and range tracking. Many missions operate with only a single frequency or with dual frequency only on the downlink transmission. In these cases, alternative calibration schemes are required.

One such alternative, referred to as DRVID (Differenced Range Versus Integrated Doppler), uses the equal but opposite effect on group delay and phase delay [19]. The integrated Doppler provides a measure of range change between two consecutive range measurements. The difference of these two data types yields a direct measure of the change in $2k/f^2$ between the two measurement times, thereby providing information on $\dot{k}$. Thus, DRVID provides a means for calibrating the Doppler data. Its effectiveness has been limited, however, by operational constraints and the accuracy of the DSN ranging system [20]. With present-day ranging equipment, the best one can expect is an accuracy of 40 cm over the Doppler count time.[6]

Another method for calibrating signal delays due to Earth's ionosphere involves tracking the dual-frequency L-band signals emitted by the GPS. For elevations above 10 deg, GPS calibrations of line-of-sight TEC have a root-mean-square (rms) accuracy of about 5×10^{16} el/m^2 or 3 cm at X-band [21] (see Section 3.4). After these calibrations are applied, Doppler observables at X-band contain residual fluctuations, caused by the ionosphere, of about 1 cm over 10 min.

Microwave tracking signals from deep space are also delayed by Earth's neutral atmosphere. The refractive effect of the troposphere results in approximately 2 m of signal-path delay at zenith and 20 m at 6-deg elevation. If second- and third-order effects due to bending are ignored, the tropospheric delay can be expressed as the sum of the contributions from the dry and the wet components of the atmosphere [22]. Thus, the one-way slant range correction is approximately

$$\Delta\rho = \Delta\rho_d + \Delta\rho_w \tag{3.3-14a}$$

where

$$\Delta\rho_{w/d} = z_{w/d} F_{w/d}(E) \tag{3.3-14b}$$

$z_{w/d}$ is the wet/dry zenith delay, E is the elevation angle, and $F_{w/d}(E)$ is the corresponding elevation-dependent mapping function, which is approximately given

[6] D. W. Green, personal communication, Honeywell Technology Solutions, Inc., Pasadena California, May 2000.

by 1/sin *E*. The currently preferred mapping function is credited to Niell [23]. It is acknowledged to be competitive with the best models, but has the added advantage of requiring no real-time meteorological data [24]. Tropospheric delay calibrations for radiometric data are obtained by applying the mapping function for the elevation of the ray path to an independently provided estimate of zenith delay. The dry component contributes about 95% of the total zenith delay and is proportional to the surface pressure. Under normal meteorological conditions, the dry portion is close to static equilibrium and is calculated to an accuracy of a few millimeters from measurements of surface barometric pressure, using the Saastamoinen model as improved by Elgered [24,25]. The wet portion, on the other hand, is proportional to the water vapor density along the ray path and is highly unstable [26]. Models of the static component of the wet troposphere based on local meteorological data are typically accurate to only about 4 cm at zenith [24].

Total zenith delays accurate to a centimeter or better are provided by the GPS calibration system described in Section 3.4 [27]. Once these delays are separated into wet and dry components, using surface weather data in conjunction with the Elgered model to infer the dry delay, the individual wet and dry components are mapped to the appropriate spacecraft line of sight. Zenith-delay measurement errors are magnified in this calculation by approximately 1/sin *E*, such that accuracies at 10 deg of elevation are on the order of 6 cm. More accurate calibration in the line-of-sight path delay to a spacecraft, especially at lower elevations, may require direct line-of-sight measurements such as those obtained from a narrow beamwidth water vapor radiometer (WVR) [28] or a Fourier-transform spectrometry (FTS) instrument [29].

The DSN has implemented a new generation of WVR in support of the Cassini Gravitational Wave Experiment, which is scheduled to begin in December 2001. Recent tests with two of these WVRs on the 21-km baseline at the Goldstone Deep Space Communications Complex indicate that differential atmospheric delay fluctuations can be measured to an accuracy of between 0.2 to 0.5 mm over time scales of 10 s to 10,000 s [30]. These results translate into an Allan variance that meets the Cassini stability requirements [30].

3.3.4 Platform Parameters

The quantities that define the locations of the tracking stations in the adopted inertial reference frame are referred to as platform parameters. These parameters may be divided into three distinct subsets: (a) the positions of tracking sites on Earth's crust; (b) the orientation angles of the crust relative to Earth's instantaneous axis of rotation and the equinox of date; and (c) the orientation angles of the instantaneous pole and equinox of date in the inertial reference frame.

3.3.4.1 Station Locations. The location of a DSN tracking antenna is defined as a reference point on the antenna's stationary axis [31]. For an

antenna with intersecting axes, the station location is defined as the point at which the two axes intersect. If the secondary axis is offset from the primary axis by a distance, b, the station location is defined as that point on the primary axis where the secondary axis would intersect if b were zero. These conventions give rise to model corrections to the recorded data that are carefully applied in the data analysis [4,31].

The coordinates of stations are expressed in the Conventional International Origin (CIO) 1903.0 terrestrial reference system. In this system, the z-axis is the 1903.0 standard pole. The x-axis points toward the 1903.0 meridian of Greenwich, and the y-axis completes the right-handed system, with positive y being 90 deg east. Station coordinates, as illustrated in Fig. 3-1, are defined as r_s (spin radius), λ_s (longitude measured easterly from Greenwich) and z_s (height above the equator).

It can be seen from Eq. 3.2-1 that Doppler-determined angles are highly sensitive to errors in station location components r_s and λ_s. A longitude error maps one-for-one into spacecraft right ascension, while an error in r_s results in a spacecraft declination error of

$$\Delta\delta = \frac{\Delta r_s}{r_s} \cot \delta \tag{3.3-15}$$

Since the planetary orbits about the Sun lie very nearly in the ecliptic plane, this error can be approximated as

$$\Delta\delta > 2\frac{\Delta r_s}{r_s} \tag{3.3-16}$$

Thus, an error of 5 cm in r_s translates into an error of at least 20 nrad in the Doppler-inferred declination.

Since the early 1980s, the vectors between many of the DSN stations (that is, the relative station locations) have been precisely determined by VLBI measurements of natural radio sources (see Chapter 4). Vector baselines have been determined to about 2 cm [32]. Changes in baseline lengths of a few centimeters per year have been measured to an accuracy of 1 to 2 mm per year [33].

The VLBI measurements provide accurate information on relative station positions, but must be coupled with other measurement techniques in order to tie the locations to the geocenter. Data from GPS and satellite laser ranging (SLR) are sensitive to geocenter location through the satellite dynamics. These data provide estimates of station locations accurate to the centimeter level [34,35]. Folkner [36] has utilized available VLBI, GPS, and SLR station location estimates, together with precise local surveys between collocated stations, to determine a subset of DSN station locations accurate in a geocentric reference frame to 3 cm, or better, in each component. Locations of newer DSN antennas were determined to an accuracy of 5 to 9 cm, using a combination of

GPS measurements and conventional survey. With additional effort in the local survey, these stations could also be located to the centimeter level, if such accuracy were required. The locations are given in the International Terrestial Reference Frame ITRF93, a frame consistent with Earth-orientation calibrations delivered to navigation teams [35,36]. Measurements of continental drift provided by VLBI and/or GPS permit the needed corrections for station motion since the 1993 epoch [36]. Corrections are also made for the effects of solid Earth tides, ocean loading, and pole tide, which are significant at the centimeter level [4].

3.3.4.2 Earth Orientation. The orientation of the terrestrial reference frame relative to the instantaneous axis of rotation and the equinox of date can be defined by three quantities, commonly referred to as X and Y pole location parameters and UT, or UT1 – UTC, a correction to time of day. The Y parameter is a right-handed rotation about the x-axis of the 1903.0 CIO frame. The X parameter is a subsequent rotation about the y-axis. The UT correction is then applied to compute the Greenwich hour angle of the true equinox of date [4,31]. The X and Y polar motion parameters are also referred to as PMX and PMY, respectively.

Polar motion, the motion of the solid Earth with respect to Earth's spin axis, has been measured for more than 100 years. It consists principally of circular oscillations with amplitudes of 100 and 200 mas (milliarcseconds) and periods of about one year and 433 days, respectively. In addition, there is a long-term drift of a few milliarcseconds per year. Decade time-scale variations have also been observed with amplitudes of 50 mas [37]. Rapid polar motion, fluctuating on time scales of a few weeks to a few months, has been measured with peak-to-peak variations of less than 20 mas [38]. The total effect of these variations produces excursions in the pole location of 10 m over a period of one year [39] as illustrated in Fig. 3-5. Oscillations on time scales of a year or less are believed to be driven by the atmosphere and oceans [40], while the Chandler wobble (433-day period) is possibly also excited by the atmosphere and oceans [41]. The long-term drift may be due to postglacial rebound or to melting ice in Greenland or Antarctica [42].

Earth's rate of rotation is not constant. The length of day (LOD) varies by several milliseconds over a wide range of time periods. Variations over a period of one year are illustrated in Fig. 3-6. Secular increases in LOD of about 1 ms per century are attributed to tidal dissipation of lunar forces. There are also secular effects produced by changes in the moment of inertia of the solid Earth due to the melting of ice following the ice ages [43]. Variations up to 5 ms in LOD over decadal and interannual time scales are believed to be primarily due to angular momentum transfer between Earth's solid mantle and fluid core [43]. Rapid variations on time scales of less than two years have been

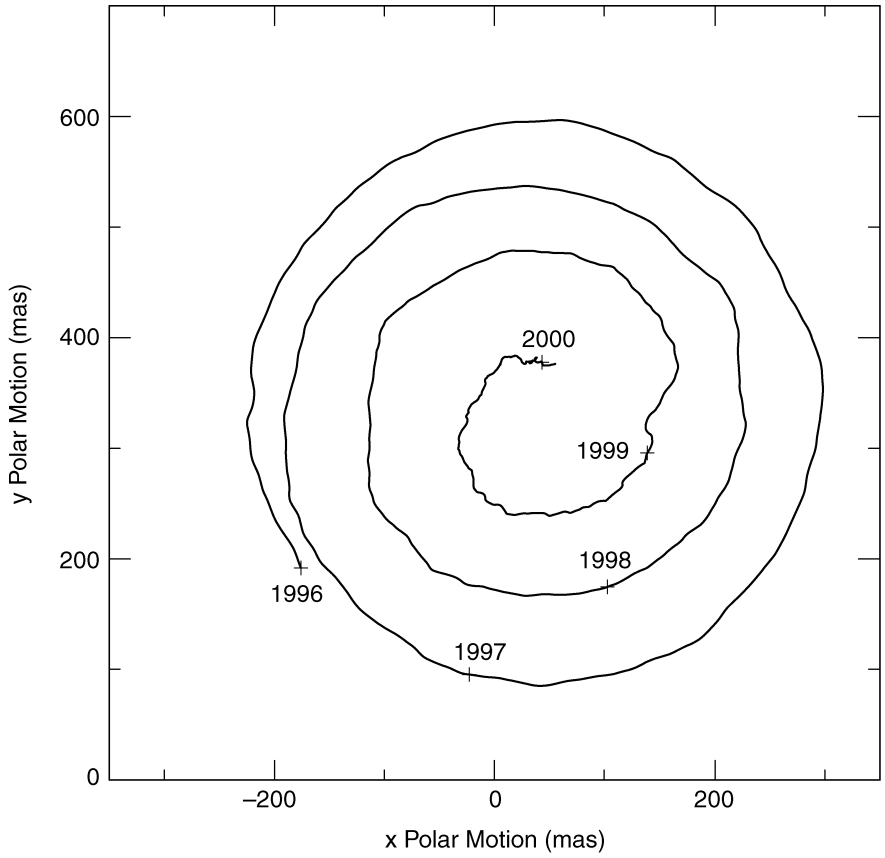

Fig. 3-5. Observed values of polar motion from January 1996 to January 2000.

shown to be highly correlated with atmospheric effects [44]. In fact, atmospheric angular momentum (AAM) data are used by the DSN to assist in determining Earth rotation time series [45].

If left uncorrected in the tracking observable models, UT and polar motion (PM) errors translate directly into spacecraft angular position errors. For example, an error of 1 ms in UT produces an error of about 70 nrad in spacecraft right ascension as determined from a single pass of Doppler data (see Eq. 3.2-1). This level of error corresponds to about 16 km at Mars.

Flight project requirements for UT and PM calibration accuracy are typically stated in terms of displacement at Earth's surface. The two polar motion parameters, PMX and PMY, have a conversion of about 3 cm per mas of rotation. The UT parameter is given in milliseconds where 1 ms translates to 46 cm of rotation at the equator.

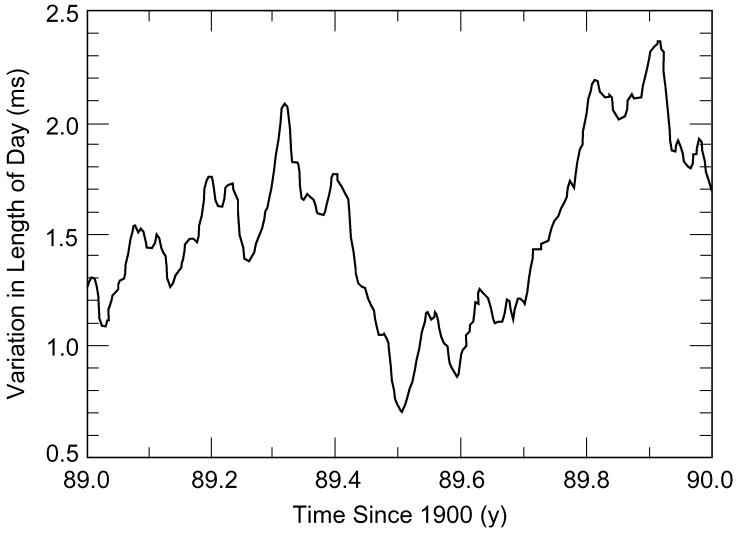

Fig. 3-6. Sample length-of-day time series.

Flight project requirements for UT and PM calibration accuracy have become more stringent during the last two decades. The Galileo Project required 30-cm prediction accuracy per component over a week, and 10-cm accuracy three weeks after the observations [46]. Mars Pathfinder, on the other hand, required 10-cm prediction accuracy over a week and 5-cm accuracy three weeks after the observations [47]. It is anticipated that a number of future projects will require near-real-time accuracies of 10 cm or better in each component.

Due to the stochastic nature of these effects and the need to calibrate navigation data in near-real time, it is necessary to generate a time series for PMX, PMY, and UT, predicting well into the future. This time series is calculated using the Kalman Earth Orientation Filter (KEOF), a program that incorporates state-of-the-art geophysical models, precise measurements from a variety of observation techniques, and stochastic models for the UT and PM parameters [48]. Measurement techniques used include the GPS, SLR, VLBI, AAM, and lunar laser ranging (LLR) [45,49].

The GPS Calibration and Tracking System (see Section 3.4) provides near-continuous measurements of PM and LOD. The epoch values of UT required for integrating the LOD measurements are obtained primarily from VLBI, and as available, from LLR. The SLR data provide additional PM estimates, while daily AAM are a good proxy for LOD. Furthermore, the AAM 5-day forecasts, obtained from numerical weather models, are valuable for generating predictions of LOD [45].

Time series from these sources are typically referenced to an internationally recognized terrestial reference frame (at present ITRF97) [34]. However, as noted in Section 3.3.4.1, navigation currently expects to receive all platform parameters referenced to ITRF93 in order to maintain consistency with the station location file now in use. Therefore, prior to KEOF processing, each of the input series is rotated, as necessary, to ITRF93.

Time series of UT and PM produced with the KEOF in the ITRF93 reference frame are delivered twice per week to navigation, with a latency of approximately one day past the data arc. During critical mission phases, deliveries may be required every day, as was the case for Mars Polar Lander during the week leading up to its scheduled encounter in 1999. These rapid-service time series, when used for near-real-time calibration on the delivery day, have one-sigma accuracies of 3 to 5 cm in PM, and 7 cm in UT. Accuracy of the predicted values degrades with time, and by 7 days, these values are 11 to 13 cm for PM and 24 cm for UT (see Fig. 3-7). After-the-fact calibrations with a 2-week delay have accuracies as good as 4 to 6 mm in each component, due to the abundance of high-quality prior measurements.[7]

Accuracies of the various time series are assessed based upon comparisons with truth series referred to as SPACE98, SPACE99, etc. [50–52].These time series are generated once per year, using the final "best" products of the various space geodetic data sources. The reference series SPACE98 is purported to have an accuracy over the last several years approaching 2 mm in each PM parameter and 6 mm in UT [51].

3.3.4.3 Precession and Nutation. The effects of lunar and solar gravitation on an oblate Earth cause the orientation of Earth's spin axis to continually change with respect to inertial space. These changes in orientation are described by a long-period rotation of the spin axis, referred to as precession, upon which is superimposed a small periodic oscillation known as nutation. Models for precession and nutation are used to rotate from "of date" coordinates at a measurement epoch to the celestial reference frame and associated epoch used by navigation to calculate spacecraft orbits. The nutation model adopted by the IAU in 1980, and used for interplanetary navigation, is deficient at about 3 to 4 mas per year [53]. A revision to this model by Mathews et al.[8] is purported to have an accuracy of 0.15 mas, based upon comparisons to VLBI observations. The new model was adopted by the IAU in August 2000.

---

[7] R. S. Gross, personal communication, Tracking Systems and Applications Section, Jet Propulsion Laboratory, Pasadena, California, April 2000.

[8] P. M. Mathews, T. A. Herring, and B. A. Buffet, "Modeling of Nutation-Precession: New Nutation Series for Nonrigid Earth, and Insights into the Earth's Interior," submitted to the Journal of Geophysical Research, 2000.

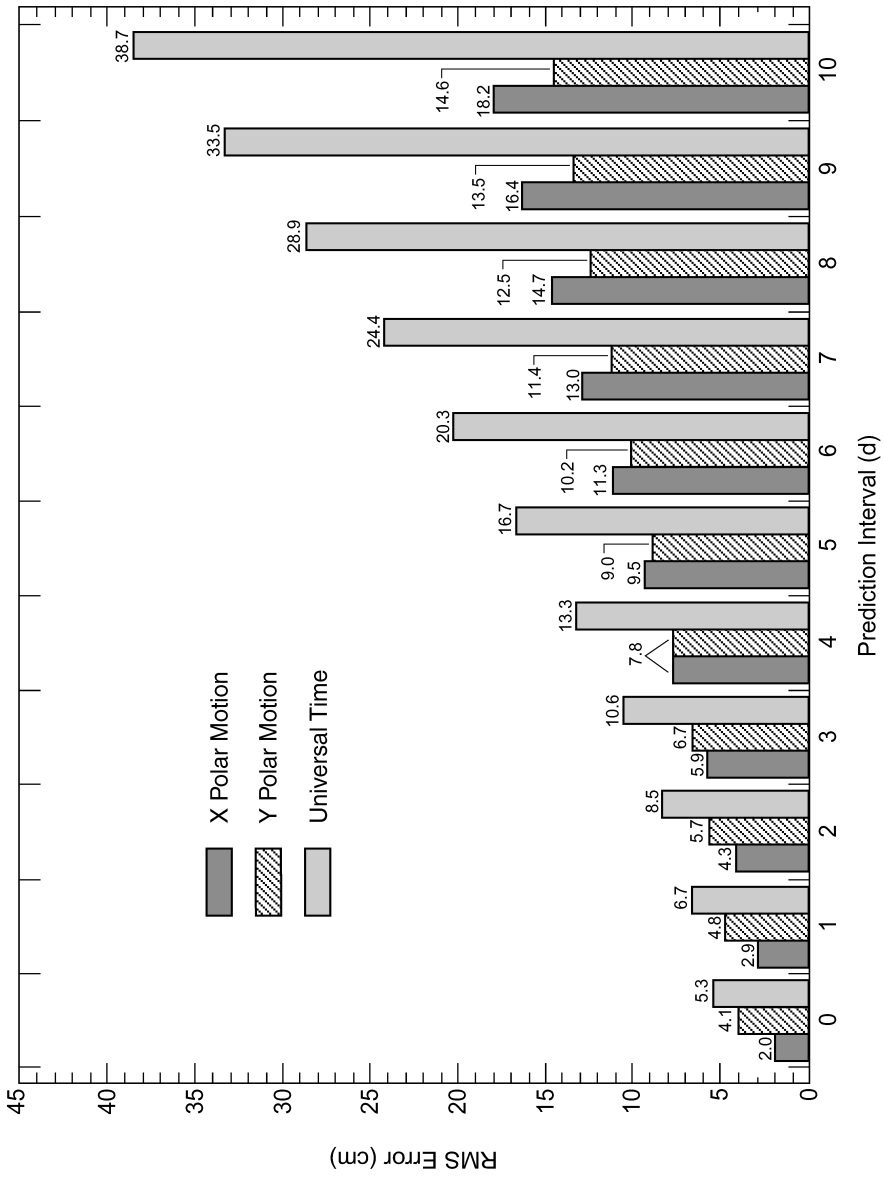

Fig. 3-7. Errors in predicted values for polar motion and universal time as a function of prediction interval past last measurement.

Corrections to the precession and nutation models used for interplanetary navigation are obtained from VLBI observations of natural radio sources [33,54]. These corrections are provided to navigation in ICRF93 (see Section 2.2), a radio reference frame consistent with ITRF93. Precession and nutation models that incorporate these corrections are accurate to 5 nrad up to a year beyond the VLBI observations [55].

The rotations for precession and nutation, following the rotations for UT and PM, yield station coordinates in the radio reference frame. A final small correction may then be required to rotate to the ephemeris frame used for navigation (see Section 4.1.3) [4].

3.4 The GPS Calibration and Tracking System

Calibration of DSN tracking data for media delays, Earth orientation, and clock offsets is largely dependent upon data from the GPS. This system consists of at least 24 satellites spaced around the globe in six orbit planes at a geocentric altitude of approximately 26,000 km. Each satellite continuously transmits dual L-band carriers (L1 = 1.2276 GHz and L2 = 1.57542 GHz) modulated with a pseudorandom noise code (P-code) from which properly equipped receivers can measure precise range and range change [56,57]. The range data are referred to as pseudorange, due to an embedded unknown clock offset between the GPS transmitter and the receiver. These clock offsets are typically modeled and accounted for in the data analysis [58,59]. Range change information is obtained from measurements of the carrier phase.

GPS satellite orbits are chosen to ensure that ground-based observers can simultaneously receive signals from at least four satellites at all times [56,57]. In reality, visibility typically is such that it is possible to receive signals from more than four satellites. Receivers designed for the high-performance applications described in this monograph are capable of concurrently tracking at least eight satellites [60]. It is this abundance of simultaneous high-precision multisatellite measurements at multiple sites that gives the GPS tracking approach its remarkable power.

GPS transmissions are under the jurisdiction of the U.S. Department of Defense (DoD). For security reasons, the DoD has implemented a number of measures designed to limit user point-positioning accuracy. These measures include encrypting (referred to as antispoofing) the precise ranging codes modulated on L1 and L2 and dithering (known as selective availability [SA]) the transmitter clocks [57]. Under SA, coarse accuracy (50 to 100 m) point positioning can be obtained with a single frequency receiver tracking the clear acquisition (CA) code modulated on L1 [61]. In the absence of SA, a user can achieve point positioning accuracy of 5 to 15 m, depending largely on corrup-

tion due to the ionosphere. As of this writing, the DoD has elected to turn off SA, a move that will significantly benefit civil GPS users.

Meanwhile, civil users with high-accuracy requirements have developed a number of means for addressing DoD security measures. These measures include codeless techniques for acquiring precise dual-frequency range and carrier phase [62–64], differential techniques or explicit clock estimation to eliminate SA effects, and utilization of ground networks to generate high-accuracy satellite orbits [59,65]. The application of these and other techniques since the early 1990s has enabled differential, stationary positioning over intercontinental distances to an accuracy of 1 cm or better [66]. Precise orbit determination for the TOPEX/Poseidon satellite, carrying a dual-frequency GPS receiver, was demonstrated in nonreal time, with an accuracy of better than 3 cm in altitude and 5 cm in the cross-track and down-track components [67]. Recent development of wide-area differential GPS systems has led to real-time transfer of GPS orbit and clock corrections to users over satellite links [68,69]. This capability will permit dual-frequency users with appropriate on-board processing capability to obtain global, instantaneous positioning with horizontal accuracy of 10 cm and vertical accuracy of 20 cm [70,71].

A major element in each of these exceptional achievements has been the use of globally distributed, geodetic-quality GPS ground receivers. The International GPS Service (IGS), a multinational organization of more than 75 contributing agencies, currently coordinates the operation of a global GPS network of approximately 200 ground receivers and seven analysis centers [72,73]. The IGS Central Bureau and one of the analysis centers are located at the Jet Propulsion Laboratory (JPL). The IGS provides tracking data, GPS satellite orbits, and other data products to a worldwide community of researchers and other users. This tracking network includes a subnet of receivers located at each DSN complex as well as the Global GPS Network (GGN), a 60-site network implemented and operated by JPL for the NASA Solid Earth and Natural Hazards Program [72]. Data from a global subset of the GGN and from the DSN are returned in a continuous stream, with latency of a few seconds, to the GPS Data Handling Facility at JPL. Latency varies for the other IGS sites, with 75% of the sites having data available within 6 hours [72].

Receivers in the IGS network are capable of codeless operation and can concurrently track at least eight satellites. A number of receivers installed since 1998 are capable of 12-satellite tracking [60]. Typical rms accuracies of the dual-frequency-combined (that is, “ionosphere-free”) measurements are 5 mm in carrier phase and 50 cm in pseudorange when operating in the codeless mode [66]. These accuracies are sufficient to meet the requirements for DSN tracking-data calibrations [59].

Calibration accuracy requirements for navigation tracking data can be satisfied with GPS data from at least 12 sites having uniform global distribution

[59,74]. An automated GPS calibration system has been implemented by the DSN to process on a daily basis all available data acquired during the preceding 27 hours from approximately 21 stations. These 21 sites include receivers at each DSN complex and a globally distributed subset of the IGS network. Calibrations are generated on 5-minute time intervals and are made available in tabular form within 12 hours after the last data are recorded.

The GPS calibration system utilizes dual-frequency range and carrier-phase measurements from the 21 sites to determine GPS orbits, Earth orientation, offsets between clocks, site-dependent tropospheric delays, and a number of other secondary parameters [59]. These calculations are performed with Gipsy-Oasis II, a least-squares estimation program developed for high-accuracy geodesy and satellite orbit determination [75]. The estimated Earth orientation parameters are PMX, PMY, and LOD. An unambiguous value for UT cannot be obtained from GPS alone, since a rotation of the stations in longitude cannot be distinguished from a corresponding rotation of the satellite constellation. However, data from VLBI provide monthly, unambiguous measurements of UT to an accuracy of 0.02 ms (0.9 cm) [52,76]. The GPS calibrations are tied to the ITRF97 [34,76], through the use of six fiducial stations whose locations are held fixed at the ITRF97 values in the least-squares filter. Table 3-2 gives the accuracies of these calibrations.

Table 3-2. Accuracies for the GPS rapid-service calibrations.

Physical Parameters	Calibration Accuracy
Earth orientation, PMX, and PMY	0.3–0.4 mas (1 cm) [77]
LOD	0.03 ms (1.4 cm)[a]
Zenith troposphere delay	< 1 cm [78]

[a]R. S. Gross, personal communication.

This performance enables the timely delivery of KEOF files and troposphere files at the requisite accuracy for navigation (see Sections 3.3.4.2 and 3.3.3).

Clock offsets between GPS receivers at DSN sites are estimated in the daily rapid-service processing to a precision of 100 psec [77]. However, embedded in these estimates are differential delays through the GPS antennas, cabling between those antennas and the GPS receivers, and more significantly, the GPS receiver electronics. Tests performed in 1989 demonstrated that these delays could be calibrated to better than 1 ns through such procedures as zero-baseline tests and traveling clocks.[9] Moreover, variations in these delays can

[9]L. E. Young, personal communication, Tracking Systems and Applications Section, Jet Propulsion Laboratory, Pasadena, California, May 2000.

be controlled to well below 1 ns by the use of quality cabling and a thermally controlled environment for the receivers [79]. It is therefore possible to implement the capability for determining intercomplex clock offsets to an accuracy of 1 ns or better. However, the current tie between the GPS receiver clock and the local station clock to which spacecraft tracking is referenced is not good to this level, and path delays through the instrumentation used for spacecraft tracking are not calibrated to this level. The GPS calibration system, with proper links to the station clocks, would be capable of delivering nanosec inter-complex timing information for navigation should a requirement for this capability materialize. The current GPS rapid-service calibration system could make clock synchronization information available on a daily basis. In addition, the advent of real-time GPS data retrieval and processing suggests the future possibility of nanosecond-precision clock synchronization in near-real time [70]. However, in order to realize the full navigation benefits of this timing information, it will be necessary to improve calibration accuracy for instrumental path delays in the spacecraft tracking equipment. Today, for example, station instrumental path delays can only be calibrated to this level by observations of natural radio sources. Since instrumental delays vary with time, it is necessary to perform these calibrations at the time of radiometric measurements.

Dual-frequency measurements from GPS satellites are also used to calibrate spacecraft signals for ionospheric delays. The P2−P1 observable, derived from pseudorange measurements of the P-code on the L1 and L2 downlinks, provides an absolute measure of the ionospheric delay between the receiver and satellite, but contains more multipath and system noise than the carrier-phase data. The differenced pseudorange measurements also contain biases due to interfrequency delays in receiver and satellite hardware. These delays are nearly constant over several days and can be estimated or separately calibrated [80,81]. The L1−L2 phase-based observable provides a more precise measure of the ionospheric delay, but contains an unknown bias resulting from carrier-cycle ambiguity. The combination of these measurements yields a highly precise time history of TEC along the line of sight to each GPS satellite.

Calibrations for deep space tracking signals require the application of an algorithm to map the TEC values obtained from the GPS measurements to the appropriate spacecraft line of sight. As currently implemented, the algorithm assumes that the ionosphere can be represented as a single thin shell located at an altitude of 450 km above Earth's surface. TEC measurements between the GPS satellites and each DSN complex are used to determine the local shell characteristics, from which ionospheric delays to a particular spacecraft line of sight are calculated. Accuracy of this local thin-shell approach has been assessed at approximately 5 TEC units (TECU) (or 3 cm at X-band) for DSN tracking of spacecraft above 10 deg elevation [21]. Accuracy can be as good as

3 TECU at moderate to high elevations and as bad as 7 to 8 TECU below 10 deg [21].

A global ionosphere mapping technique, referred to as GIM, is under development and promises to provide a more robust and accurate method for spacecraft calibration [21,82–84]. GIM utilizes worldwide TEC measurements from IGS network data to characterize a global ionosphere having three layers [85]. When GIM is fully operational (circa 2002), accuracies of DSN ionospheric calibrations are expected to improve by as much as a factor of two for spacecraft at low-elevation angles. Thus, calibration accuracies of 3 to 5 TECU should be achieved over the entire range of elevation [83,85].

3.5 Range and Doppler System Measurement Performance

The effects of all significant measurement errors on range and Doppler tracking observables have been described in previous sections. These error sources are summarized in Table 3-3. The evolution of tracking capabilities is illustrated by estimating system performance for three cases: (a) 1980 radiometric tracking at S-band, (b) the 1992 system operating at X-band, and (c) the current (2000) system operating at X-band. Error contribution due to thermal noise depends on spacecraft telecommunication parameters and is a function of the distance from the tracking station to the spacecraft; typical values are given in Table 3-3.

Tracking at a single-frequency band in the two-way mode has been assumed for each case. Dual-frequency downlinks, which are available from some spacecraft, can be used to reduce the effects of the ionosphere and solar plasma. For example, solar plasma delays exceeding 200 m in S-band Viking Lander range measurements were calibrated to about 8-m accuracy using dual S and X downlinks from the Viking orbiters [86,87]. Today, spacecraft operate primarily with an X-band uplink and downlink. Plasma effects for an X-band two-way link are reduced by a factor of 13 when compared to an S-band link. Future use of Ka-band two-way links would reduce this effect by an additional factor of 14.

For the current system, the random error of 0.03 mm/s for an X-band Doppler measurement made over 60 s is due primarily to fluctuations in solar plasma density along the line of sight. This value varies with proximity of the ray path to the Sun and with the solar cycle. The random error for a range measurement is due primarily to thermal noise.

A range observable, being an absolute measure of distance, is sensitive to measurement biases as well as random errors. For moderate Sun-Earth-probe angles, the accuracy of the current system is limited by knowledge of delays through station and spacecraft electronics. This instrument bias is about 2 m.

Table 3-3. Radiometric measurement system error characteristics.

Error Source	Magnitude		
	1980 S-Band	1992 X-Band	2000 X-Band
Random error for 60-s average			
Doppler	1 mm/s	0.03 mm/s	0.03 mm/s
Range	200 cm	60 cm	60 cm
Instrument bias (range)	5 m	5 m	2 m
Instrument stability @ 8 h	10^{-13}	10^{-14}	10^{-14}
Station locations			
Spin radius	100 cm	10 cm	3 cm
Longitude	100 cm	10 cm	3 cm
Baseline components	30 cm	5 cm	2 cm
Earth orientation (1-d prediction)	100 cm	30 cm	7 cm
Earth orientation (after the fact)	20 cm	3 cm	1 cm
Troposphere			
Zenith bias	4.5 cm	4.5 cm	1 cm
Line-of-sight fluctuation (over 10 min at 15-deg elevation)	1 cm	1 cm	1 cm
Ionosphere (line of sight, above 10 deg)	100 cm	3 cm	3 cm
Solar plasma			
20-deg Sun-Earth-probe angle			
Total line of sight	229 m	17 m	17 m
Drift over 8 h	15 m	115 cm	115 cm
Station-differenced	7 cm	0.5 cm	0.5 cm
180-deg Sun-Earth-probe angle			
Total line of sight	16 m	116 cm	116 cm
Drift over 8 h	2 m	15 cm	15 cm
Station-differenced	1 cm	0.1 cm	0.1 cm
Station clock			
Epoch	1 μs	1 μs	1 μs
Rate	10^{-12}	5×10^{-14}	5×10^{-14}
Stability @ 1000 s	10^{-14}	10^{-15}	10^{-15}

Antenna multipath, media fluctuations, and instrumental delay variations introduce systematic effects over time scales varying from seconds to hours, but the magnitudes of these effects are less than the instrument bias by a factor of at least two [88].

Doppler performance for navigation is assessed by looking at the accumulation of range error over a station tracking pass. The current system error with the largest magnitude is due to fluctuations in solar plasma delay along the line of sight. At X-band, the plasma delay drift over an 8-h pass varies from as little as 1 m at solar opposition to 20 m or higher at Sun-Earth-probe angles of 20 deg or less. But this error, being of random signature, may not degrade the spacecraft state estimate as seriously as the more systematic, few-centimeter-level errors that arise from uncertainties in platform parameters.

3.6 Range and Doppler System Positioning Performance

For the last several decades, navigation has relied primarily upon the Doppler and range systems for Earth-based tracking [89]. As previously noted, several days of Doppler are sufficient to determine an interplanetary orbit, at least in benign geometries and well-modeled force fields. Unfortunately, there are situations where Doppler tracking alone can lead to erroneous estimates of spacecraft position. For example, determination of spacecraft declination from a 12-h pass of Doppler, weighted at 0.1 mm/s, is typically accurate to about 50 nrad to 100 nrad for $\delta = 23$ deg [90]. However, the sensitivity of a single Doppler pass to errors in declination is proportional to sin δ, which vanishes at $\delta = 0$ (see Eq. 3.2-1). Thus, as a spacecraft passes through zero declination, a longer Doppler arc is needed, or tracking must be supplemented with an alternative technique for measuring angles [91,92]. Long arcs of Doppler and range data can, under favorable conditions, provide angular position accuracy of 40 nrad or better [55].

Determination of spacecraft angular position from Doppler and range data may also be severely degraded by inaccurately modeled forces such as spacecraft gas leaks, thruster firings, or solar radiation pressure. These forces are difficult to model since they are influenced by unknown, but significant, stochastic terms [93]. The integrity of the modeling is important because range, right ascension, and declination are not directly measured by the Doppler observable, but instead are weakly determined from signatures in the observables. For example, any unmodeled effects that alter the amplitude and/or phase of the diurnal signature in the data may be interpreted by the estimator as changes in spacecraft declination and/or right ascension (see Eq. 3.2-1). Moreover, these inferred changes may be quite large relative to actual perturbations

in the trajectory induced by the unmodeled forces. Consider, for example, the simplified example [94] shown in Fig. 3-8. In this example, a 5-m perturbation in range to the spacecraft is interpreted by the estimator as a 1000-km shift in the lateral, or plane-of-sky, position. In this case, the estimator is constrained by dynamical models to straight-line motion. The unmodeled accelerations cause a deviation from the modeled path of 5 m in the geocentric range direction. The estimator, given precise knowledge of geocentric range and constrained to straight-line motion, will adjust the value of the less-certain lateral position parameter in order to minimize the data residuals. Since the angular position parameters are weakly determined from the Doppler and range data, large changes in these parameter values may be required to reduce the data residuals and remove the observed signature. In the cited example, a range change of 5 m at a distance of 10^8 km translates to 1000 km in plane-of-the-sky displacement.

This hypothetical example illustrates the sensitivity of weakly determined parameters to mismodeled forces and demonstrates that solving for the orbit parameters from Doppler and range data alone can be highly risky. As this example shows, large errors in weakly determined position parameters can result from unmodeled forces on the spacecraft, particularly if those forces move the spacecraft in a direction that is well-determined. Specifically, erroneous force models conspired with precise range knowledge to produce a large and incorrect displacement in the estimate of spacecraft angular position. This example also illustrates the frequently encountered discrepancy between orbits

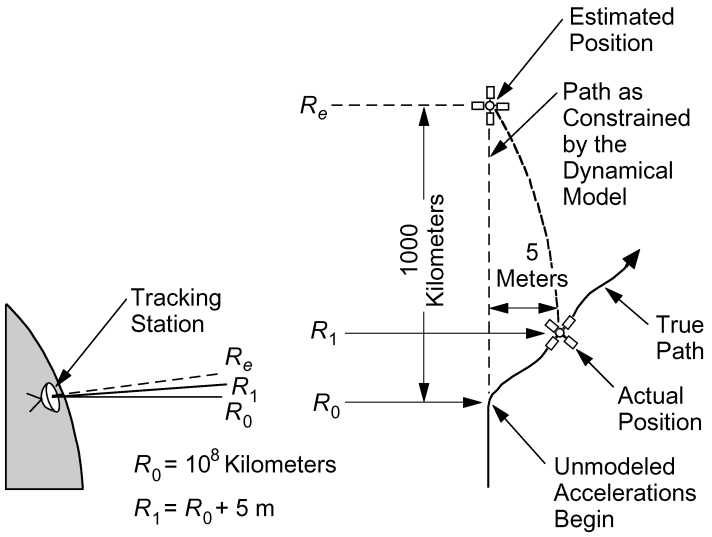

Fig. 3-8. Illustration of orbit-determination errors resulting from mismodeled dynamics, poorly measured angles, and the use of precise ranging.

determined with Doppler only and those obtained from Doppler and precise range measurements. Ironically, in the presence of mismodeled forces, less accurate or no range data can result in a more accurate orbit estimate [95]. The optimum resolution to this dilemma is not the deweighting or discarding of the range data, but rather the incorporation of appropriate stochastic models for spacecraft motion into the data-analysis software. Sequential least-squares filters have been successfully applied to estimation problems of this type for more than two decades [96]. These filters effectively deweight the dynamic constraints by allowing stochastic accelerations to be modeled and estimated. But the key to obtaining highly accurate orbit solutions is the proper utilization of data that provide a direct and accurate measure of all three components (r, α, δ) of spacecraft position.

These three components of position can also be measured using only the DSN ranging system. Simultaneous reception of ranging signals from two complexes during view period overlaps can provide a measure of angular position. This data type is referred to as differenced two-way and three-way range and is illustrated in Fig. 3-9. Differenced range was developed for the Voyager mission as a means of measuring declination to an accuracy of 1 μrad at the Saturn low-declination encounters [89]. The limiting errors for these observables are uncalibrated biases due to clock offsets and different instrumental delays at the two stations, currently as high as 1 μs (300 m). The required 6.4-m differenced range accuracy (equivalent to 600 nrad on the Goldstone-to-Canberra baseline) was

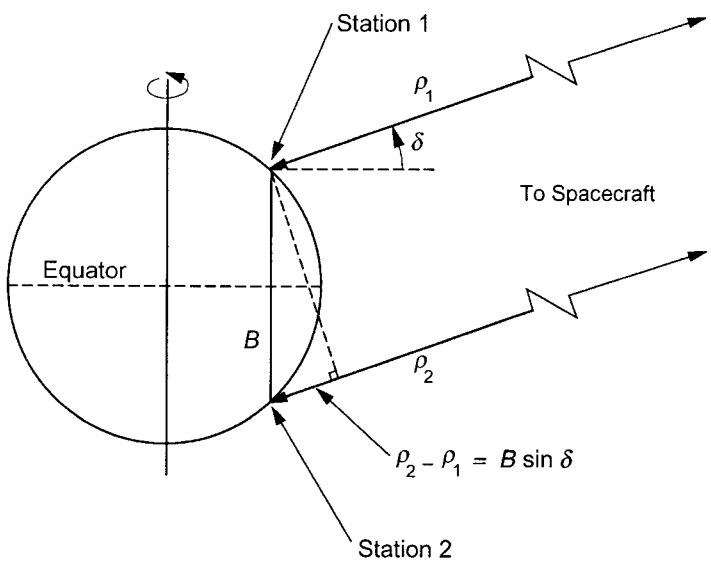

Fig. 3-9. Differenced simultaneous range from two stations, providing a measure of spacecraft angular position.

achieved instead with differenced near-simultaneous two-way range [95]. This data type is operationally difficult due to the round-trip light time and the uplink handover from one station to another. Furthermore, as the time between two-way measurements increases, the differenced observables are increasingly contaminated by uncalibrated space plasma and other line-of-sight delay variations. These problems were especially acute for the Voyager S-band ranging system, and following the Saturn encounter, the project decided to no longer acquire near-simultaneous range data [95].

Analysis in the early 1990s of two-way range and Doppler (S-band uplink and X-band downlink) data from the Ulysses spacecraft just prior to the Jupiter encounter suggested that range accuracies of a few meters were achievable [97]. This analysis also indicated that observations of this quality from two or more DSN complexes could provide spacecraft declination to 200 nrad in low declination (4 to 8 deg) situations. Improvements in range calibrations (see Table 3-3) have enabled some reduction in these angular errors. However, future missions requiring high-accuracy (50 nrad, or better) angles from Earth-based tracking will rely upon VLBI technology.

For a planetary orbiter, the motion of the spacecraft about the planet induces a strong signature in the Doppler received at Earth. The planet-relative position of the spacecraft may be recovered from analysis of this signature over one or more revolutions. However, the orientation of the orbit plane about the line of sight from Earth to the planet is not determined as accurately as the other components of state. This orientation component may be directly observed by either Doppler data acquired simultaneously at two stations and then differenced, or by interferometric delay-rate measurements [98]. For two spacecraft in orbit about the same planet, which may be observed simultaneously in the same beamwidth of Earth-based tracking antennas, differential measurements may dramatically improve orbit accuracy for both spacecraft, as discussed in Chapter 5.

References

[1] N. F. deGroot, “Radio Frequency Selection and Radio Interference Prevention,” chapter in *Deep Space Telecommunications Systems Engineering* (J. H. Yuen, editor), New York: Plenum Press, 1983.

[2] J. C. Breidenthal and T. A. Komarek, “Radio Tracking System,” chapter in *Deep Space Telecommunications Systems Engineering* (J. H. Yuen, editor), New York: Plenum Press, 1983.

[3] J. B. Berner et al., “Regenerative Pseudo-Noise Ranging for Deep Space Applications,” *TMO Progress Report 42-137*, vol. January–March 1999,

http://tmo.jpl.nasa.gov/progress_report/issues.html Accessed October 16, 2000.

[4] T. D. Moyer, *Formulation for Observed and Computed Values of Deep Space Network Data Types*, JPL Publication 00-7, Jet Propulsion Laboratory, Pasadena, California, October 2000.

[5] T. W. Hamilton and W. G. Melbourne, "Information Content of a Single Pass of Doppler Data from a Distant Spacecraft," *Space Programs Summary 37-39, Vol. III, The Deep Space Network*, Jet Propulsion Laboratory, Pasadena, California, pp. 18–23, May 31, 1966.

[6] D. W. Curkendall and S. R. McReynolds, "A Simplified Approach for Determining the Information Content of Radio Tracking Data," *Journal of Spacecraft and Rockets*, vol. 6, no. 5, pp. 520–525, May 1969.

[7] P. F. Kuhnle, "NASA/JPL Deep Space Network Frequency and Timing," *Proceedings of the Twenty-first Annual Precise Time and Time Interval (PTTI) Applications and Planning Meeting*, Redondo Beach, California, pp. 479–490, November 28–30, 1989.

[8] J. A. Barnes et al., "Characterization of Frequency Stability," *IEEE Transactions on Instrumentation and Measurement*, vol. IM-20, no. 2, pp.105–120, May 1971.

[9] J. S. Border and E. R. Kursinski, "Deep Space Tracking and Frequency Standards," *Proceedings of the IEEE 45th Annual Symposium on Frequency Control*, IEEE 91CH2965-2, Los Angeles, California, pp. 594–607, May 29–31, 1991.

[10] C. E. Dunn, S. M. Lichten, D. C. Jefferson, and J. S. Border, "Subnanosecond GPS-Based Clock Synchronization and Precision Deep-Space Tracking," *TDA Progress Report 42-111*, vol. July–September 1992, http://tmo.jpl.nasa.gov/progress_report/issues.html Accessed October 16, 2000.

[11] L. E. Young et al., "Formation of a GPS-Linked Global Ensemble of Hydrogen Masers and Comparison to JPL's Linear Ion Trap," *Proceedings of the 1996 IEEE International Frequency Control Symposium*, Honolulu, Hawaii, pp. 1159–1162, June 5–7, 1996.

[12] D. C. Jefferson, S. M. Lichten, and L. E. Young, "A Test of Precision GPS Clock Synchronization," *Proceedings of the 1996 IEEE International Frequency Control Symposium*, Honolulu, Hawaii, pp. 1206–1210, June 5–7, 1996.

[13] G. J. Dick, R. T. Wang, and R. L. Tjoelker, "Cryo-Cooled Sapphire Oscillator with Ultra-high Stability," *Proceedings of the 1998 IEEE International Frequency Control Symposium*, Pasadena, California, pp. 528–533, May 27–29, 1998.

[14] R. L. Tjoelker, J. D. Prestage, and L. Maleki, "Record Frequency Stability with Mercury in a Linear Ion Trap," *Proceedings of the Fifth Symposium on Frequency Standards and Metrology,* Woods Hole, Massachusetts, pp. 33–38, October 15–19, 1995.

[15] G. J. Dick and R. T. Wang, "Cryo-Cooled Sapphire Oscillator for the Cassini Ka-band Experiment," *Proceedings of the 1997 IEEE International Frequency Control Symposium,* Orlando, Florida, pp. 1009–1014, May 28–30, 1997.

[16] *Deep Space Network/Flight Project Interface Design Handbook, Vol. 1: Existing DSN Capabilities,* JPL 810-5, Module TRK-30, Rev. E, http://eis.jpl.nasa.gov/deepspace/dsndocs/810-005/ Accessed November 6, 2000.

[17] R. Woo and J. W. Armstrong, "Spacecraft Radio Scattering Observations of the Power Spectrum of Electron Density Fluctuations in the Solar Wind," *Journal of Geophysical Research,* vol. 84, no. A12, pp. 7288–7296, December 1, 1979.

[18] W. A. Coles and J. K. Harmon, "Propagation Observations of the Solar Wind Near the Sun," *The Astrophysical Journal,* vol. 337, no. 2, pp. 1023–1034, February 1989.

[19] P. F. MacDoran, "A First-Principles Derivation of the Differenced Range Versus Integrated Doppler (DRVID) Charged Particle Calibration Method," *Space Programs Summary 37-62, Vol. II, The Deep Space Network,* Jet Propulsion Laboratory, Pasadena, California, pp. 28–34, March 1970.

[20] D. W. Green, V. W. Lam, and H. N. Royden, "Effects of the Charged Particle Environment on Voyager Navigation at Jupiter and Saturn," AIAA 80-1650 paper presented at the AIAA/AAS Astrodynamics Conference, Danvers, Massachusetts, August 11–13, 1980.

[21] C. M. Ho, B. D. Wilson, A. J. Mannucci, U. J. Lindqwister, and D. N. Yuan, "A Comparative Study of Ionospheric Total Electron Content Measurements and Models with TOPEX," *Radio Science,* vol. 32, no. 4, pp. 1499–1512, July–August 1997.

[22] G. E. Lanyi, "Tropospheric Delay Effects in Radio Interferometry," *TDA Progress Report 42-78,* vol. April–June 1984, http://tmo.jpl.nasa.gov/progress_report/issues.html Accessed October 16, 2000.

[23] A. Niell, "Global Mapping Functions for the Atmospheric Delay at Radio Wavelengths," *Journal of Geophysical Research,* vol. 101, no. B2, pp. 3227–3246, February 10, 1996.

[24] V. de Brito Mendes, "Modeling the Neutral-Atmosphere Propagation Delay in Radiometric Space Techniques," University of New Brunswick [Canada] Technical Report 199, April 1999.

[25] G. Elgered, "Tropospheric Radio Path Delay From Ground-Based Microwave Radiometry," *Atmospheric Remote Sensing by Microwave Radiometry* (M. Janssen, editor), New York: Wiley & Sons, 1992.

[26] R. N. Treuhaft and G. E. Lanyi, "The Effect of the Dynamic Wet Troposphere on Radio Interferometric Measurements," *Radio Science*, vol. 22, no. 2, pp. 251–265, March–April 1987.

[27] S. M. Lichten, "Precise Estimation of Tropospheric Path Delays with GPS Techniques," *TDA Progress Report 42-100*, vol. October–December 1989, http://tmo.jpl.nasa.gov/progress_report/issues.html Accessed October 16, 2000.

[28] A. B. Tanner, "Development of a High-Stability Water Vapor Radiometer," *Radio Science*, vol. 33, no. 2, pp. 449–462, March–April 1998.

[29] R. Beer, *Remote Sensing by Fourier Transform Spectrometry*, New York: John Wiley & Sons, 1992.

[30] G. M. Resch et al., "Calibration of Atmospherically Induced Delay Fluctuations Due to Water Vapor," NASA/CP-2000-209893, *International VLBI Service for Geodesy and Astrometry, 2000 General Meeting Proceedings* (N. R. Vandenberg and K. D. Baver, editors), Kötzting, Germany, pp. 274–279, February 21–24, 2000.

[31] O. J. Sovers and C. S. Jacobs, *Observation Model and Parameter Partials for the JPL VLBI Parameter Estimation Software MODEST—1996*, JPL Publication 83-39, Rev. 6, Jet Propulsion Laboratory, Pasadena, California, August 1996.

[32] J. A. Steppe, S. H. Oliveau, and O. J. Sovers, "Earth Rotation Parameters from DSN VLBI: 1995," in *Earth Orientation, Reference Frames and Atmospheric Excitation Functions Submitted for the 1994 IERS Annual Report: IERS Technical Note 19* (P. Charlot, editor), pp. R21–R27, Paris: Observatoire de Paris, September 1995.

[33] C. S. Jacobs et al., "The JPL Extragalactic Radio Reference Frame: Astrometric Results of 1978–96 Deep Space Network VLBI," *TMO Progress Report 42-133*, vol. January–March 1998, http://tmo.jpl.nasa.gov/progress_report/issues.html Accessed October 16, 2000.

[34] C. Boucher, Z. Altamimi, and P. Sillard, *The 1997 International Terrestrial Reference Frame (ITRF97): IERS Technical Note 27*, Paris: Observatoire de Paris, May 1999.

[35] C. Boucher, Z. Altamimi and L. Duhem, *Results and Analysis of the ITRF93: IERS Technical Note 18,* Paris: Observatoire de Paris, October 1994.

[36] W. M. Folkner, "DSN Station Locations and Uncertainties," *TDA Progress Report 42-128,* vol. October–December 1996, http://tmo.jpl.nasa.gov/progress_report/issues.html Accessed October 16, 2000.

[37] K. Lambeck, *The Earth's Variable Rotation,* New York: Cambridge University Press, 1980.

[38] T. M. Eubanks et al., "Causes of Rapid Motions of the Earth's Pole," *Nature,* vol. 334, no. 6178, pp. 115–119, July 14, 1988.

[39] R. Hide, "Rotation of the Atmospheres of the Earth and Planets," *Philosophical Transactions of the Royal Society, Series A,* vol. 313, no. 1524, pp. 107–121, November 27, 1985.

[40] J. M. Wahr, "The Effects of the Atmosphere and Oceans on the Earth's Wobble; I, Theory," *Geophysical Journal of the Royal Astronomical Society,* vol. 70, no. 2, pp. 349–372, 1982.

[41] R. S. Gross, "The Excitation of the Chandler Wobble," *Geophysical Research Letters,* vol. 27, no. 15, pp. 2329–2332, August 1, 2000.

[42] J. M. Wahr, "Geophysical Aspects of Polar Motion, Variations in Length of Day, and the Luni-solar Nutations," chapter in *Space Geodesy and Geodynamics* (A. J. Anderson and A. Cazenave, editors), London: Academic Press, 1986.

[43] K. Lambeck, "Geophysical Geodesy," chapter in *The Slow Deformation of the Earth,* Oxford: Clarendon Press, 1988.

[44] R. Hide and J. O Dickey, "Earth's Variable Rotation," *Science,* vol. 253, no. 5020, pp. 629–637, August 9, 1991.

[45] A. P. Freedman et al., "The Short-term Prediction of Universal Time and Length of Day Using Atmospheric Angular Momentum," *Journal of Geophysical Research,* vol. 99, no. B4, pp. 6981–6996, April 1994.

[46] *Support Instrumentation Requirements Document for the 1989 Galileo Project,* Galileo Project Document 625-501, Rev. A, JPL D-476, Rev. A (internal document), Jet Propulsion Laboratory, Pasadena, California, May 1, 1988.

[47] *Mars Pathfinder Project Policies and Requirements Document,* JPL D-10856, Rev. C (internal document), Jet Propulsion Laboratory, Pasadena, California, January 1995.

[48] D. D. Morabito, T. M. Eubanks, and J. A. Steppe, "Kalman Filtering of Earth Orientation Changes," chapter in *The Earth's Rotation and Refer-*

ence Frames for Geodesy and Geodynamics (A. K. Babock and G. A. Wilkins, editors), pp. 257–267, IAU, 1988.

[49] R. S. Gross et al., "A Kalman-Filter-Based Approach to Combining Independent Earth-Orientation Series," *Journal of Geodesy,* vol. 72, no. 4, pp. 215–235, April 1998.

[50] R. S. Gross, "Combinations of Earth Orientation Measurements: SPACE97, COMB97, and POLE97," *Journal of Geodesy,* vol. 73, no. 12, pp. 627–637, February 2000.

[51] R. S. Gross, *Combinations of Earth Orientation Measurements: SPACE98, COMB98, and POLE98,* JPL Publication 99-6, Jet Propulsion Laboratory, Pasadena, California, April 1999.

[52] R. S. Gross, *Combinations of Earth Orientation Measurements: SPACE99, COMB99, and POLE99,* JPL Publication 00-5, Jet Propulsion Laboratory, Pasadena, California, April 2000.

[53] T. A. Herring, C. R. Gwinn, and I. I. Shapiro, "Geodesy by Radio Interferometry: Studies of the Forced Nutations of the Earth, Part 1: Data Analysis," *Journal of Geophysical Research,* vol. 91, no. B5, pp. 4745–4754, April 10, 1986.

[54] C. Ma et al., "The International Celestial Reference Frame as Realized by Very Long Baseline Interferometry," *The Astronomical Journal,* vol. 116, no. 1, pp. 516–546, July 1998.

[55] J. A. Estefan and W. M. Folkner, "Sensitivity of Planetary Cruise Navigation to Earth Orientation Calibration Errors," *TDA Progress Report 42-123,* vol. July–September 1995, http://tmo.jpl.nasa.gov/progress_report/issues.html Accessed October 16, 2000.

[56] J. J. Spilker, Jr., "GPS Signal Structure and Performance Characteristics," *Global Positioning System,* ION 0-936406-00-3, pp. 29–54, 1980.

[57] B. W. Parkinson and J. J. Spilker, Jr., editors, *Global Positioning System: Theory and Applications, Volume I,* Progress in Astronautics and Aeronautics, vol. 163, AIAA, 1996.

[58] B. W. Parkinson and J. J. Spilker, Jr., editors, *Global Positioning System: Theory and Applications, Volume II,* Progress in Astronautics and Aeronautics, vol. 164, AIAA, 1996.

[59] S. M. Lichten, "Estimation and Filtering for High-Precision GPS Applications," *Manuscripta Geodaetica,* vol. 15, pp. 159–176, 1990.

[60] International GPS Service, http://igscb.jpl.nasa.gov/igscb/station/general/rcvr_ant.tab Accessed September, 12, 2000.

[61] J. F. Zumberge and W. I. Bertiger, "Ephemeris and Clock Navigation Message Accuracy," chapter in *Global Positioning System: Theory and*

Applications, Volume I (B. W. Parkinson and J. J. Spilker, Jr., senior editors), Progress in Astronautics and Aeronautics, AIAA, 1996.

[62] R. R. Hatch, R. Keegan, and T. A. Stansell, "Kinematic Receiver Technology for Magnavox," *Sixth International Geodetic Symposium on Satellite Positioning,* Columbus, Ohio, pp. 174–183, March 17–20, 1992.

[63] T. K. Meehan et al, "The TurboRogue Receiver," *Sixth International Geodetic Symposium on Satellite Positioning,* Columbus, Ohio, pp. 209–218, March 17–20, 1992.

[64] J. B. Thomas, *Signal Processing Theory for the TurboRogue Receiver,* JPL Publication 95-6, Jet Propulsion Laboratory, Pasadena, California, April 1, 1995.

[65] C. L. Thornton, S. M. Lichten, L. E. Young, and T. P. Yunck, "Novel Concepts for Precise Low Earth Orbiter Navigation with GPS," IAF-97-M.6-01, 48th International Astronautical Congress, Turin, Italy, October 6–10, 1997.

[66] G. Blewitt et al., "Global Coordinates with Centimeter Accuracy in the International Terrestrial Reference Frame Using GPS," *Geophysical Research Letters,* vol. 19, no. 9, pp. 853–856, May 4, 1992.

[67] W. I. Bertiger et al., "GPS Precise Tracking of TOPEX/Poseidon: Results and Implications," *Journal of Geophysical Research: Oceans,* vol. 99, no. C12, pp. 24449–24464, December 15, 1994.

[68] J. Ceva, "Hughes Aircraft's Architectural Design of the Federal Aviation Administration Wide Area Augmentation System: An International System," IAF-97-M6.04, 48th International Astronautical Congress, Turin Italy, October 6–10, 1997.

[69] W. I. Bertiger et al., "A Real-time Wide Area Differential GPS System," *Journal of Navigation,* vol. 44, no. 4, pp. 433–447, Winter 1997.

[70] R. J. Muellerschoen, W. I. Bertiger, M. F. Lough, D. Stowers, and D. Dong, "An Internet-Based Global Differential GPS System, Initial Results," Institute of Navigation, *2000 National Technical Meeting,* Anaheim, California, pp. 220–225, January 26–28, 2000.

[71] R. J. Muellerschoen, W. I. Bertiger, and M. F. Lough, "Results of an Internet-Based Dual-Frequency Global Differential GPS System," *IAIN World Congress in Association with the U.S. ION 56th Annual Meeting,* San Diego, California, pp. 796–802, June 26–28, 2000.

[72] *International GPS Service for Geodynamics 1998 Annual Report,* JPL 400-839, Jet Propulsion Laboratory, Pasadena, California, July 1999.

[73] R. E. Neilan, J. F. Zumberge, G. Beutler, and J. Kouba, "The International GPS Service: A Global Resource for GPS Applications and Research,"

ION-GPS-97, Kansas City, Missouri, pp. 883–889, September 16–19, 1997.

[74] U. J. Lindqwister, S. M. Lichten, and E. S. Davis, "The GPS TOPEX/Poseidon Precise Orbit Determination Experiment: Implications for Design of GPS Global Networks," IAF-93-A.5.38, 44th Congress of the International Astronautical Federation, Graz, Austria, October 16–22, 1993.

[75] F. H. Webb and J. F. Zumberge, editors, *An Introduction to Gipsy/Oasis II*, JPL D-11088 (internal document), Jet Propulsion Laboratory, Pasadena, California, July 1993.

[76] *1998 IERS Annual Report*, Paris: Observatoire de Paris, 1999.

[77] R. J. Muellerschoen, S. M. Lichten, U. J. Lindqwister, and W. I. Bertiger, "Results of an Automated GPS Tracking System in Support of TOPEX/Poseidon and GPSMet," *ION GPS-95*, Palm Springs, California, pp. 183–193, September 12–15, 1995.

[78] Y. E. Bar-Sever, P. M. Kroger, and J. A. Borjesson, "Estimating Horizontal Gradients of Tropospheric Path Delay with a Single GPS Receiver," *Journal of Geophysical Research*, vol. 103, no. B3, pp. 5019–5035, March 10, 1998.

[79] G. Petit et al., "Use of GPS Ashtech Z12T Receivers for Accurate Time and Frequency Comparisons," *IEEE Transactions on Ultrasonics, Ferroelectrics and Frequency Control*, vol. 46, no. 4, pp. 941–949, July 1999.

[80] G. E. Lanyi and T. Roth, "A Comparison of Mapped and Measured Total Ionospheric Electron Content Using Global Positioning System and Beacon Satellite Observations," *Radio Science*, vol. 23, no. 4, pp. 483–492, July–August 1988.

[81] B. D. Wilson and A. J. Mannucci, "Extracting Ionospheric Measurements from GPS in the Presence of Anti-Spoofing," *ION GPS-94*, Salt Lake City, Utah, pp.1599–1608, September 20–23, 1994.

[82] A. J. Mannucci et al., "A Global Mapping Technique for GPS-Derived Ionospheric Total Electron Content Measurements," *Radio Science*, vol. 33, no. 3, pp. 565–582, May–June 1998.

[83] B. A. Iijima et al., "Automated Daily Process for Global Ionospheric Total Electron Content Maps and Satellite Ocean Altimeter Ionospheric Calibration Based on Global Positioning System Data," *Journal of Atmospheric and Solar-Terrestrial Physics*, vol. 61, no. 16, pp. 1205–1218, November 1, 1999.

[84] W. Ross Stone, editor, *Review of Radio Science 1996–1999*, IEEE PC5838, August 1999.

[85] A. J. Mannucci et al., "Assessment of Global TEC Mapping Using a Three-Dimensional Electron Density Model," *Journal of Atmospheric and Solar-Terrestrial Physics,* vol. 61, no. 16, pp. 1227–1236, November 1, 1999.

[86] R. D. Reasenberg et al., "Viking Relativity Experiment: Verification of Signal Retardation by Solar Gravity," *The Astrophysical Journal,* vol. 234, no. 3, pp. L219–L221, December 15, 1979.

[87] R. W. Hellings et al., "Experimental Test of the Variability of G Using Viking Lander Ranging Data," *Physical Review Letters,* vol. 51, no. 18, pp. 1609–1612, October 31, 1983.

[88] L. E. Young, "Improved Ranging Systems," *Workshop on Relativistic Gravitation Experiments in Space,* NASA CP 3046, Annapolis, Maryland, pp. 203–205, June 28–30, 1989.

[89] J. F. Jordan and L. J. Wood, "Interplanetary Navigation: An Overview," *The Journal of the Astronautical Sciences,* vol. 32, no. 1, pp. 17–28, January–March 1984.

[90] T. McElrath, "Ulysses Orbit Determination at High Declinations," *Flight Mechanics/Estimation Theory Symposium, 1995,* NASA CP 3299, Goddard Space Flight Center, Greenbelt, Maryland, pp. 227–287, May 16–18, 1995.

[91] D. W. Curkendall, "Radiometric Technology for Deep Space Navigation: A Development Overview," AIAA 78-1395, paper presented at the AIAA/AAS Astrodynamics Conference, Palo Alto, California, August 7–9, 1978.

[92] V. J. Ondrasik and K. H. Rourke, "Application of Quasi-VLBI Tracking Data Types to the Zero Declination and Process Noise Problems," AAS 71-399, paper presented at the AAS/AIAA Astrodynamics Specialist Conference, Fort Lauderdale, Florida, August 17–19, 1971.

[93] T. H. Taylor et al., "Orbit Determination for the Voyager II Uranus Encounter," AIAA 86-2112, *Astrodynamics Conference,* Williamsburg, Virginia, pp. 178–191, August 18–20, 1986.

[94] W. G. Melbourne, "Navigation Between the Planets," *Scientific American,* vol. 234, no. 6, pp. 58–74, June 1976.

[95] T. H. Taylor et al., "Performance of Differenced Range Data Types in Voyager Navigation," *TDA Progress Report 42-71,* vol. July–September 1982, http://tmo.jpl.nasa.gov/progress_ report/issues.html Accessed October 16, 2000.

[96] C. S. Christensen and S. J. Reinbold, "Navigation of the Mariner 10 Spacecraft to Venus and Mercury," *Journal of Spacecraft and Rockets,* vol. 12, no. 5, pp. 280–286, May 1975.

[97] S. W. Thurman, T. P. McElrath, and W. M. Pollmeier, "Short-Arc Orbit Determination Using Coherent X-Band Ranging Data," AAS 92-109, *Advances in the Astronautical Sciences, Volume 79, Part 1* (R. E. Diehl et al., editors), proceedings of the AAS/AIAA Spaceflight Mechanics Meeting, Colorado Springs, Colorado, pp. 23–44, February 24–26, 1992, San Diego, California: Univelt, 1992.

[98] S. R. Poole, M. P. Ananda, and C. E. Hildebrand, "Radio Interferometric Measurements for Accurate Planetary Orbiter Navigation," *Advances in the Astronautical Sciences, Volume 40, Part 1* (P. Penso et al., editors), proceedings of the AAS/AIAA Astrodynamics Specialist Conference, Provincetown, Massachusetts, pp. 93–111, June 25–27, 1979, San Diego, California: Univelt, 1980.